

Topology Preserving Maps – Extracting Layout Maps of Wireless Sensor Networks from Virtual Coordinates

Dulanjalie C. Dhanapala and Anura P. Jayasumana
Department of Electrical and Computer Engineering,
Colorado State University, Fort Collins, CO 80523, USA

Abstract— A method for obtaining Topology Preserving Maps (TPM) from Virtual Coordinates (VCs) of wireless sensor networks is presented. In a Virtual Coordinate System (VCS), a node is identified by a vector containing its distances, in hops, to a small subset of nodes called anchors. Layout information such as physical voids, shape and even relative physical positions of sensor nodes with respect to X-Y directions are absent in a VCS description. Proposed technique uses Singular Value Decomposition to isolate dominant radial information and to extract topological information from VCS for networks deployed on 2-D/3-D surfaces and in 3-D volumes. The transformation required for TPM extraction can be generated using the coordinates of a subset of nodes, resulting in sensor network friendly implementation alternatives. TPMs of networks representing a variety of topologies are extracted. Topology Preservation Error (E_{TP}), a metric that accounts for both the number and degree of node flips is defined and used to evaluate 2-D TPMs. The techniques extract TPMs with E_{TP} less than 2%. Topology coordinates provide an economical alternative to physical coordinates for many sensor networking algorithms.

Index Terms— Topology-Preserving Map, Virtual Coordinates, Localization, Routing, Singular Value Decomposition, Wireless Sensor Network

I. INTRODUCTION

VIRTUAL coordinates provide an economical alternative to geographical coordinates for routing and self-organization of large-scale Wireless Sensor Networks (WSNs). Geographical coordinate based protocols such as Geographical Routing (GR) require physical location of nodes, which may be obtained by GPS or a localization algorithm. Use of GPS is infeasible or too costly for many applications, while localization using analog measurements such as signal strength and time delay is difficult and prone to errors [19][25][26][30]. Signal strength is susceptible to noise, fading and interferences due to multipath and other devices. Need for accurate power control and signal strength measurements contribute to increased hardware complexity as well as cost. Routing is carried out using directional information derived from Geographic Coordinates (GCs), and hence concave physical voids in the network degrade the performance of GR schemes. Anchor-based Virtual Coordinate Systems (VCS) characterize each node by a coordinate vector consisting of the shortest path hop distances to a set of anchors[5][6][24][27][23]. These anchors are a set

of ordinary sensor nodes with no additional capabilities. Coordinates can be obtained using a controlled/organized flooding mechanism [20] initiated by the anchors. VCS is a higher dimensional abstraction of a partial connectivity map of sensors. It has several properties, such as ease of generation, and facilitating connectivity based routing without the need for geographical information [5]-[8][25], that make it attractive for large-scale or resource-starved WSNs. The number of anchors becomes network's dimensionality in the virtual coordinate (VC) space. As the network's connectivity information is embedded in VCs, the physical voids become transparent in the Virtual Space (VS). However, VCs lose the directional information related to node positions. The number of anchors required and their placement for a given network play a crucial role in the performance of VC based routing. However, identification of the optimal number of anchors and proper anchor placement remain major challenges. Under-deployment of anchors causes identical node coordinates, while their over deployment and improper placement worsen the local minima problem causing logical voids[6].

Many disadvantages associated with VCS in comparison to geographical coordinate systems are due to the lack of information about the physical network topology and layout. As each virtual ordinate propagates radially away from an anchor, the directional information of a node with respect to the anchor is lost. Thus the physical layout information such as physical voids, relative physical direction information of sensor nodes with respect to X-Y positions, and even explicit connectivity information among pairs of nodes are absent in a VCS description. The above information can be revealed if the physical map is available. Having both, partial connectivity information that is embedded in VCs and position or direction information as in geographical coordinates can be used to overcome the disadvantages in each other's domains. However, physical topological information has to be generated without inheriting the disadvantages associated with obtaining physical location information or localization.

Obtaining a topology map resembling the physical layout topology of a network from the set of VCs that is based only on hop distances to a small set of anchors has not been possible up to now. In this paper, we present a technique to obtain Topology Preserving Maps (TPMs) that contain the topology of a network and physical features, including its geographical voids, boundary profiles and relative Cartesian directional information. TPMs overcome many of the disadvantages of VCS compared to geographical coordinate

systems but without inheriting its disadvantages, whilst preserving all the advantages of connectivity based VCs.

A TPM is a rotated and/or distorted version of the real physical node map to account for connectivity information inherent in VCs. The topological coordinates provided by the proposed method are a good substitute for geographical coordinates for many applications that depend on connectivity and location information. In fact, the topological coordinates (TCs) in conjunction with VCs from which they are derived, have been demonstrated to be better than geographical coordinates for routing due to significantly enhanced routing performance [12]. Topology coordinate space provides an alternative that is different from virtual and physical coordinates, yet preserving the advantages of the two. Boundary node identification, event region and void detection [10], and nodes gaining network awareness [11], i.e., finding the overall shape of the network and its place in the network, are among examples of techniques that have been demonstrated to benefit from the TCs. The results presented here demonstrate the ability to determine and visualize the structural characteristics of large-scale WSNs in both 2-D and 3-D. Ability to do such visualization without the need for analog measurement capability at nodes will be invaluable for networks whose nodes are extremely limited in capability, e.g., large-scale nanosensor networks [1]. Even though we focus on WSN context here, the technique is applicable to a broader class of networks.

Next, Section II reviews the background. After presenting the SVD based method for obtaining TPMs in Section III, we also refine the method to reduce its complexity. A performance evaluation metric for topology maps is presented in Section IV. In Section V, we discuss the results of three alternatives for TPM generation, with different computational and communication complexities. Section VI addresses implementation issues. Finally, Section VII discusses the future work and concludes our work.

II. BACKGROUND

We briefly review the related work on coordinate systems, and localization techniques for generating GCs and maps, for which proposed TPMs are a competitive, economical alternative. The term TPMs has been used in contexts outside sensor networking, such as multi-dimensional data organization. Though some of them are not directly applicable to WSNs, we review the most relevant ones to place the proposed scheme in context.

A. Geographic Routing (GR) vs. Virtual Coordinate Routing (VCR)

In geographic routing, the physical location of nodes is used for node addressing as well as for routing. A packet is forwarded in the direction of the destination, and thus GR gets disrupted by geographical voids. Concave voids are especially difficult to overcome. Greedy Perimeter Stateless Routing (GPSR)[14] makes greedy forwarding decisions till it fails, for example due to a geographical void, and attempts to recover by routing around the perimeter of the void. Greedy Other Adaptive Face Routing (GOAFR) [16] is a geometric ad-hoc algorithm combining greedy forwarding and face routing to overcome the local minima issue. Greedy Path Vector Face Routing with Path Vector Exchange GPVFR/PVEX [18] is similar to [16] but it requires network's planar graph.

VC based schemes, where each node is characterized by a coordinate vector corresponding to hop distances to a set of anchors, uses a distance measure in VCS to identify the node for packet forwarding. VCR scheme in [27], e.g., uses all the perimeter nodes as anchors. When a packet reaches a local minima, an expanding ring search is performed until a closer node is found or TTL expires. In VC assignment protocol (VCap), the coordinates are defined based on hop distances [5]. At local minima, VCR causes a packet to follow a rule called "local detour". In Logical Coordinate based Routing (LCR) [6], backtracking is used when greedy forwarding fails at a local minimum. Aligned VC system (AVCS) [21] re-evaluates VCs by averaging a node's own coordinate with neighboring coordinates in an attempt to overcome local minima. Convex Subspace Routing [8] overcomes the local minima by using a subset of anchors for routing, and by dynamically changing the subset to provide a convex distance surfaces for routing. In Axis-Based VC Assignment Protocol (ABVCap) [33], each node extracts a 5-tuple VC corresponding to longitude, latitude, ripple, up, and down. Existing VCR protocols rely mainly on Greedy forwarding, followed by a backtracking scheme to overcome the local minima issue. Geo-Logical Routing (GLR) [12] is a novel scheme that combines the advantages of VCS and TPM proposed in this paper to overcome disadvantages of each other's domain, thus impressively outperforming existing VCR schemes as well as GPSR which requires physical coordinates.

B. Localization

We focus on relative localization techniques, as global localization is realizable through relative localization and the actual positions of a subset of nodes or physical anchors. Centralized and distributed algorithms are available for relative localization. Distributed algorithms use Received Signal Strength Indication (RSSI), radio hop count, time difference of arrival, and/or angle of arrival for relative localization. RSSI uses signal strength to estimate the distance between nodes while radio hop count uses hop distance. The latter uses a probabilistic correction equation to approximate the hop distance to real distance [2][32]. Disadvantages of RSSI measurements include sensitivity to terrain [26] and large variations due to fading and interference. Relationship between RSSI and distance is very difficult to predict indoors [19] as well as in complex outdoor environments due to absorption and reflection of signals and propagation characteristics over different terrains. No robust and scalable algorithms are available for localization of nodes deployed on surfaces of complex 3-D structures. An RSSI measurement based distributed algorithm using triangulation for localization of 2D and 3D WSNs is proposed in [35].

Centralized algorithms for localization of 2-D networks include Semidefinite Programming (SDP) and MDS-MAP [2][29]. The former algorithm develops geometric constraints between nodes, represents them as linear matrix inequalities (LMIs), and then simply solves for the intersection of the constraints. Unfortunately, not all geometric constraints can be expressed as LMIs which preclude the algorithm's use in practice. MDS-MAP uses Multi-Dimensional Scaling (MDS) based on connectivity information.

The localization scheme in [17] first selects a subset of boundary nodes as landmarks. Next, Delaunay triangles are

generated based on Voronoi cells formed with landmarks. Finally, the network layout is discovered based on the landmarks' locations. Boundary nodes need to be identified accurately without physical information and an incremental algorithm is required to combine the Delaunay triangles.

Factors that contribute to errors in localization include inaccuracies in distance estimate, the position calculation and the localization algorithm [25]. How the localization error propagates and accumulates in a network is illustrated in [25] in terms of geographic distribution of the error, correlation, mean error and probability distribution of the error. This study shows that routability of GR with GEAR [34] falls significantly and the percentage of deliveries to wrong destinations increase as the error in localization increases.

As both VCS and topology maps are generated based on the hop distances, they are not affected by fading or signal strengths. Further, they do not rely on analog measurements such as RSSI or time delay, and thus do not have cumulative errors that affect the performance as the networks scale.

C. Mapping schemes for networks and data

TPMs discussed in this paper deviate from the localization maps. The relative localization schemes expect the relative distances to be accurate. Thus given the absolute position of a subset of nodes, global localization is realizable. In contrast, in topology maps what is important is the topology preservation, not the physical distances. The derived topology should be homeomorphic (topologically isomorphic) to the physical layout of the sensor network, i.e., between two topological spaces there has to be a continuous inverse function. In our case, it is a mapping, which preserves the topological properties of the physical network topology.

In the context of analysis of high-dimensional data, unsupervised learning algorithms have been proposed that use eigenvalue decomposition for obtaining a lower dimensional embedding of the data. Here we discuss four such schemes: Multi-Dimensional Scaling (MDS), Local Linear Embedding (LLE), Isomap and Laplacian Eigenmaps (LE)[3]. None of these methods is designed for, nor is suitable for resource starved WSNs.

Multi-Dimensional Scaling (MDS) [29][31] is a commonly used statistical technique in information visualization for exploring similarities or dissimilarities in higher dimensional data from the complete distance matrix (similarity matrix) D , which is defined as the matrix of all the pair-wise distances between points/nodes. $D = [d_{ij}]_{N \times N}$, where, N is the number of nodes in the network and d_{ij} is the distance from node i to node j with $d_{ij} = d_{ji}, \geq 0$ and $d_{jj} = 0$. In general d_{ij} can be any distance metric, but there is a possibility for the algorithm to fail if d_{ij} is not the Euclidean distance. Generating D based on hop distances requires all the nodes in a WSN to serve as anchors, an extremely expensive proposition that calculates and stores information about the distances between each pair of nodes. If such information were available at each node, 100% routing can be achieved just by following the ordinate corresponding to the destination, i.e., without the need for the topology map. MDS is therefore not practical or applicable for generating TPMs of WSN. Our novel method, based on Singular Value Decomposition (SVD), generates topology

maps of 2-D and 3-D networks, using a set of M anchors, where $M \ll N, N$ being the number of nodes.

Isomaps [32] is an extension of MDS to geodesic distance based topology map generation. Again, the geodesic distances are actual distances among nodes, which require expensive error prone distance estimators such as RSSI or Time-of-Arrival (TOA). Furthermore, if a node has the information of entire network, 100% routability is achievable without need for topology map. Moreover, LLE and LE both use an iterative approach to preserve the neighborhood distances, realization of which is infeasible in an energy limited WSNs.

All the four schemes rely highly on physical distances between all the possible pairs of nodes, and thus require localization approaches. Accuracy of both central and distributed implementations of localization is highly sensitive to channel fading and signal to noise ratio (SNR).

TABLE I. NOTATIONS USED IN THE TEXT

Notation	Description
\mathcal{N}	Set of nodes
$N= \mathcal{N} $	Number of network nodes
$n_i \in \mathcal{N}$	Node i
$\mathcal{A} \subset \mathcal{N}$	Set of anchor nodes
$M = \mathcal{A} (M \ll N)$	Number of anchors
$A_i \in \mathcal{A}, i = 1:M$	i^{th} anchor
$h_{n_i n_j}$	Minimum hop distance between nodes n_i, n_j
$P_{N \times M}$	Virtual coordinate matrix of the entire network
$P_{(i)} = [h_{n_i A_1}, \dots, h_{n_i A_M}]$	VCs of Node n_i
$Q_{R \times M}; R \ll N$	VCs of a subset of nodes
$P_{SVD}^{(i)}$	i^{th} principle component of P
$[X_T, Y_T],$	Topological coordinate matrix of a 2-D network
$[X_T, Y_T, Z_T]$	Topological coordinate matrix of a 3-D network
$[X_T, Y_T]_{(i)}$ $= [X_{T,i}, Y_{T,i}]$	Topological coordinates of node n_i of a 2-D network
$[X_T, Y_T, Z_T]_{(i)}$ $= [X_{T,i}, Y_{T,i}, Z_{T,i}]$	Topological coordinates of node n_i of a 3-D network
$[X_p, Y_p],$	Physical coordinates of a 2-D network
$[X_p, Y_p, Z_p]$	Physical coordinates of a 3-D network

III. TOPOLOGY PRESERVING MAPS FOR 2-D AND 3-D WSNs

A novel technique for obtaining a Topology Preserving Map (TPM) representation of a sensor network from its VC set is presented next. The objective is to characterize each node with a (x, y) coordinate pair, or (x, y, z) in case of 3-D WSNs, that results in a TPM that is homeomorphic to the

network's physical layout, and preserves information about node connectivity, physical layout and physical voids. We emphasize that the map so obtained is not the physical map but is a distorted version resembling it, which takes the connectivity into account. The metromap of a metro system vs. its actual physical map drawn to scale can be considered analogous to the TPM vs. physical map relationship. The metromap, though it does not have the exact physical dimensions, is in fact much more useful for the purpose of navigation. Similarly, the TPMs have been shown elsewhere to be much more effective for many sensor network related functions, e.g., routing [12], boundary detection [10], and achieving node awareness [11]. In fact, the topology coordinates (TCs) of TPM can be used as a substitute for GCs in many GC based algorithms.

Subsection A develops the technique by starting with the VCs of all the nodes to obtain a TPM. Subsection B discusses the extension of TPMs to 3-D networks. A significantly more efficient version of the technique that uses information of only a small subset of nodes to evaluate the transformation matrix is presented in Subsection C. Finally, Subsection D proposes a method of calculating node's Cartesian coordinates with lower computational complexity. Notations used in the text are summarized in Table I.

A. 2-D topology preserving maps from VCs

Consider a 2-D sensor network with N nodes and M anchors. Thus, each node is characterized by a VC vector of length M . Let P be the $N \times M$ matrix containing the VCs of all the nodes, i.e., the i^{th} row corresponds to the M -long VC vector of the i^{th} node, and j^{th} column corresponds to the virtual ordinate of all the nodes in the network with respect to j^{th} anchor. Therefore,

$$P = [h_{n_i A_j}]$$

where, $h_{n_i A_j}$ is the hop distance from node n_i to anchor A_j . For sensor network applications, it is generally desirable to have only a small subset of nodes as anchors, i.e., $M \ll N$. A 2-D network has an M -dimensional representation under the VC transformation. The main goal thus is to extract the 2-D representation of the network from this M -D space. Singular Value Decomposition (SVD) [15] of P is denoted as

$$P = U.S.V^T \quad (1)$$

where, U, S and V are $N \times N$, $N \times M$, and $M \times M$ matrices respectively [14]. U and V are unitary matrices, i.e., $U^T U = I_{N \times N}$ and $V^T V = I_{M \times M}$. SVD extracts and packages the salient characteristics of the dataset P providing an optimal basis for P . Moreover V is an optimal basis of P^T , i.e., V spans R^M . Let us consider the Principle Components (PCs) of P

$$P_{SVD} = U.S \quad (2)$$

P_{SVD} is a $N \times M$ matrix that describes each node with a new set of M -length coordinate vectors. It gives the coordinates for the data in P under the new basis V . As S is a diagonal matrix with diagonal elements being the singular values of P arranged in their descending order, elements in S provide unequal weights on columns of U . Using the unitary property of V , it is also the projection of P on to V [15], i.e.,

$$P_{SVD} = P.V \quad (3)$$

The columns of P_{SVD} , i.e., the PC values of the VC set are arranged in the descending order of information about the original coordinate set. The 1st PC captures the highest variance of the data set, and each succeeding component has the highest variance possible under the constraint that it be orthogonal to the preceding components.

Figures 1 and 2 show for two different networks, the variation over the physical layout of the first three PCs, i.e., columns of P_{SVD} given by (3), plotted against the corresponding physical positions of the nodes. As observed in [9], the first three SVD components dominate in magnitude over the remaining PCs, which are similar to Fourier basis vectors.

The set of VCs have the connectivity information embedded in it, though it has no directional information. All the nodes that are h hops away from the j^{th} anchor have h as the j^{th} ordinate. Each ordinate propagates as a concentric circle centered at the corresponding anchor, while the angular information is completely lost. Note that the most significant ordinate based on SVD, i.e., first column of P_{SVD} shown in Fig. 1 (b)) and Fig. 2 (b), is a convex surface centered at some point within the network, thus capturing the resultant effect of the conical propagation of different anchor coordinates. As SVD provides an orthonormal basis, 2nd and 3rd ordinates are orthogonal to 1st ordinate while being perpendicular to each other as illustrated in Fig. 3. Plots of the variation of 2nd and 3rd components for the two example networks in Figures 1 and 2 illustrate this as well. Therefore the second and third columns of P_{SVD} provide a set of two-dimensional Cartesian coordinates for node positions, less encumbered by the dominant radial information in VCs, which was captured by the first column. Thus instead of the M coordinates of a row of P_{SVD} to characterize a node, the second and third columns are used as Cartesian coordinates for plotting an approximate map of the network, i.e.,

$$[X_T, Y_T] = [P_{SVD}^{(2)}, P_{SVD}^{(3)}] \quad (4)$$

where, $P_{SVD}^{(j)}$ is the j^{th} column of P_{SVD} . $[X_T, Y_T]$ is the Cartesian coordinate matrix of entire node set, i.e., its i^{th} row, $[X_T, Y_T]_{(i)}$, is used as the Cartesian coordinates of i^{th} node.

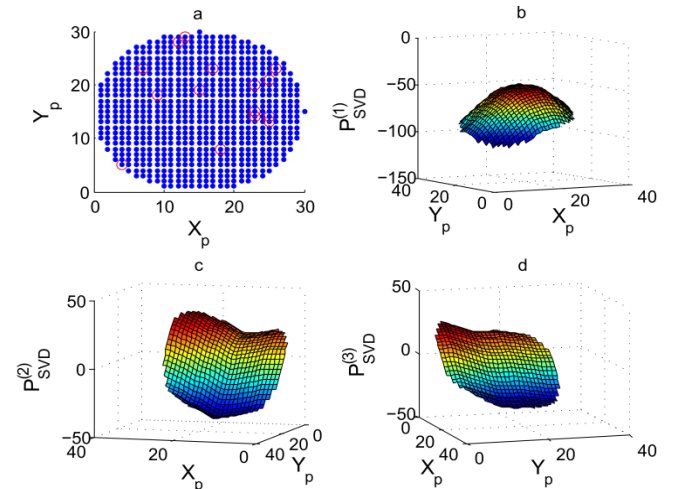


Fig. 1. a) Circular network of 707 nodes with 15 anchors, b) - d) First three PCs $P_{SVD}^{(1)}$, $P_{SVD}^{(2)}$, and $P_{SVD}^{(3)}$ plotted against the physical positions. Randomly selected anchors are marked in red circles.

We now illustrate the procedure using as an example the T-shaped network of 10 nodes shown in Figure 4 (a). Physical coordinates $[X_p, Y_p]$, and VC matrix P with respect to anchors A, C, E and J are given in Table II. SVD evaluation of P as in (1) provides V as,

$$V = \begin{pmatrix} -0.55 & -0.34 & -0.71 & -0.30 \\ -0.34 & -0.25 & 0.00 & 0.91 \\ -0.55 & -0.34 & 0.71 & -0.30 \\ -0.54 & 0.84 & 0.00 & 0.03 \end{pmatrix}$$

P_{SVD} can now be evaluated using (3), and thus topological coordinates of nodes is given by (4). $[P_{SVD}^{(2)}, P_{SVD}^{(3)}]$ is tabulated in Table II and plotted in Fig. 4(b).

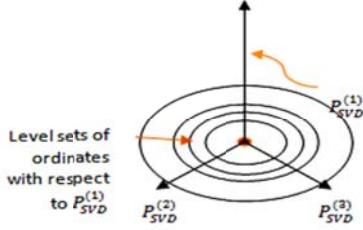


Fig. 3. Nature of principal component directions derived from VC.

A question that naturally arises is why the removal of the largest PC and keeping less significant 2nd and 3rd terms, which in many applications of PCA correspond to error or deviations, yields a good layout map. First we address why the dominant PC cannot be used. Note that our dataset consists of VCS of a network. Therefore, if we were to reconstruct the VCS using a subset of PCs, the first component would be the most important one. However, the reconstruction space we seek is an approximation to the physical layout, and the mapping from the physical layout to the acquisition space (VCS) is highly nonlinear. Each VC propagates concentrically wrt to the corresponding anchor, i.e., all the nodes at a minimum distant r from the anchor map to the value r .

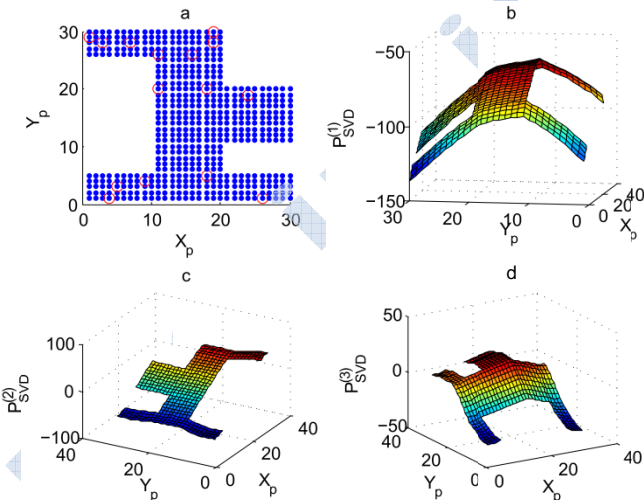


Fig. 2. a) Odd shaped network with 550 nodes with 15 anchors, b) - d) First three PCs $P_{SVD}^{(1)}$, $P_{SVD}^{(2)}$, and $P_{SVD}^{(3)}$ plotted against the physical positions. Randomly selected anchors are marked in red circles.

The impact of conical nature of propagation of each VC from the corresponding anchor and the net effect of many such anchors completely dominate over any cardinal direction information embedded in VCS. In Appendix A, we show the convexity of the first PC for a simple 1-D network and extend

the result to a 2-D network. This convex nature is also evident from Figures 1(b) and 2(b). As the first PC contains much of the dominant convex form of distortion introduced in going from physical layout to the VC space, using it as a major axis for mapping produces maps with a significant amount of folding. Appendix A also illustrates the resulting folding of the map, both for a 1-D example and the simple 2-D example of Fig. 1 (a), when the first PC is used for reconstruction.

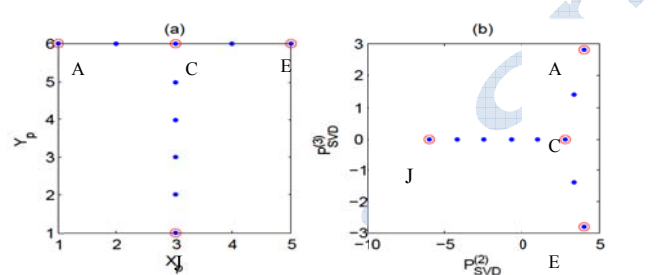


Fig. 4. a) Physical map of a T-shaped example network, and b) Topology map of the network in a).

TABLE II. PHYSICAL COORDINATES, VCS AND TOPOLOGICAL COORDINATES FOR THE NETWORK IN FIG. 4(a)

ID	X_p	Y_p	P				P_{SVD}			
			A	C	E	J	$P_{SVD}^{(1)}$	$P_{SVD}^{(2)}$	$P_{SVD}^{(3)}$	$P_{SVD}^{(4)}$
A	1	6	0	2	4	7	-6.62	4.06	2.83	0.82
B	2	6	1	1	3	6	-5.74	3.46	1.41	-0.12
C	3	6	2	0	2	5	-4.87	2.87	0.00	-1.05
D	4	6	3	1	1	6	-5.74	3.46	-1.41	-0.12
E	5	6	4	2	0	7	-6.62	4.06	-2.83	0.82
F	3	5	3	1	3	4	-5.76	1.10	0.00	-0.76
G	3	4	4	2	4	3	-6.66	-0.66	0.00	-0.47
H	3	3	5	3	5	2	-7.55	-2.43	0.00	-0.19
I	3	2	6	4	6	1	-8.45	-4.19	0.00	0.10
J	3	1	7	5	7	0	-9.35	-5.96	0.00	0.39

Based on the assertion above that the 1st PC contains much of the radial distortion introduced in physical layout to VC mapping, it follows that the removal of the 1st PC from consideration removes much of this radial information from the data set. This is evident in 2nd and 3rd PC plots in Fig. 1(c), 1(d), 2(c) and 2(d) for the two examples. The remaining PCs contain the information from the physical layout that was masked due to this convex distortion in the original VC set. Therefore, as specified in Eqn. (4), we use the next two significant components to yield the cardinal directional information to plot the layout maps. SVD based construction assures that these two components, i.e., second and third PCs, form an orthogonal Cartesian plane for network. Note that these maps are not physical layout maps; rather they are distorted maps that preserve much of the topological relationships of the network layout.

These Cartesian coordinates are estimated without having any kind of physical directional or positioning information beyond the radial information (hop distance) with respect to the anchors. Results presented later demonstrate that a TPM thus obtained preserves the topological characteristics of the original network. One can even identify features such as physical voids that were not apparent in the VC based description.

A formal general proof as to how the 2nd and 3rd PCs preserve many of the physical features of the network layout has so far eluded us. The above description is the best intuitive explanation we have based on analysis of many data sets.

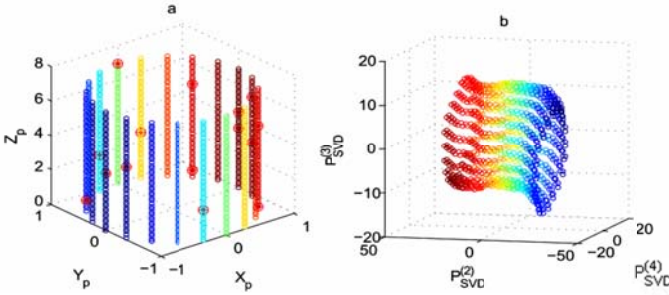


Fig. 5. a) A network on a cylindrical surface (900 nodes) Randomly selected 20 anchors are marked in red circles, and b) topology map of a).

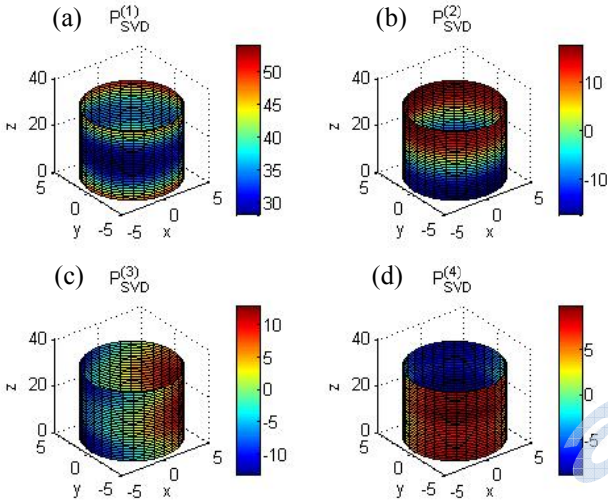


Fig. 6. First four PCs a) $P_{SVD}^{(1)}$, b) $P_{SVD}^{(2)}$, c) $P_{SVD}^{(3)}$, and d) $P_{SVD}^{(4)}$ of a cylindrical network plotted as a color map on the surface of the network.

A. 3-D topology preserving map from VCs

Sensor networks may be deployed within 3-D volumes, on 3-D surfaces, or a combination of those. Here we consider sensors deployed on a 3-D surface, which may even wrap around, thus affecting VC propagation in complex ways. Consider the uniform cylindrical surface shown in Fig. 5(a) on which 900 nodes are deployed. Fig. 6 (a)-(d) show the plots of the first four PCs for each node in the network. They are denoted by $P_{SVD}^{(1)}$, $P_{SVD}^{(2)}$, $P_{SVD}^{(3)}$, and $P_{SVD}^{(4)}$ respectively. As SVD provides an orthonormal basis, the 2nd, 3rd and 4th PCs are orthogonal to the 1st ordinate while being perpendicular to each other. Like with the 2-D case, the salient feature of the VCS, i.e., the radial propagation of coordinates is captured by the 1st PC as seen in Fig. 6(a). The value is lowest at the center of the surface and increases toward edges resulting in a convex variation along the height. Thus removing it from further consideration allows us to uncover linear patterns embedded in the VC set. As seen in Fig. 6(b), the second PC varies monotonically along the height of the cylinder, thus it can be used to obtain the Z coordinate for the topology map. More interestingly 3rd, and 4th PCs, which are taken as X and Y coordinates, directionally distribute in such a way that they

are orthogonal to each other while being normal to 2nd PC. The resulting TPM is illustrated in Fig. 5(b). TPM generation on 3-D surfaces can thus be done by ignoring the first PC, and by taking 2nd, 3rd, and 4th columns of P_{SVD} , to provide a set of three-dimensional (3-D) Cartesian coordinates.

To summarize, the topological coordinates of node n_i for the 3-D case is given by,

$$\begin{aligned} [X_T, Y_T, Z_T]_{(i)} &= [P_{SVD}^{(2)}, P_{SVD}^{(3)}, P_{SVD}^{(4)}]_{(i)} \\ &= [P_{(i)} \cdot V^{(2)}, P_{(i)} \cdot V^{(3)}, P_{(i)} \cdot V^{(4)}] \end{aligned} \quad (5)$$

where, $[P_{SVD}^{(j)}]_{(i)}$ is j^{th} PCs of node n_i . Note that the above result holds for 3-D volumes as well. The first PC in that case will propagate radially outward from the center of the volume, as opposed to the center of the area in case of 2-D networks.

B. Generation of Cartesian coordinate set using VCs of a subset of nodes

Cartesian coordinates for 2-D TPM are obtained by multiplying the node's VC by V as in (3) and (4) (and as in (5) for 3-D TPMs). V is based on P , the $N \times M$ matrix that consists of VCs of all the nodes. In sensor networks, it is crucial to reduce communication and computation overheads. This section presents a process to generate the transformation matrix V with only a small subset of rows of P , thus significantly reducing the computation overhead. Let Q be the sub-matrix of P corresponding to an appropriately selected set of R nodes (rows). Let the SVD of Q be,

$$Q = U_Q \cdot S_Q \cdot V_Q^T \quad (6)$$

Q is $R \times M$, where M is the number of anchors. U_Q , S_Q and V_Q are $R \times R$, $R \times M$ and $M \times M$ matrices respectively. If Q is selected appropriately, V_Q can serve as a substitute, or at a minimum a good approximation, for V for TPM generation. Note that V_Q has the same size as V in (1), and is also unitary. Following the same procedure as earlier, we use

$$P_{SVD} = P \cdot V_Q \quad (7)$$

The Cartesian coordinates for TPMs of 2-D and 3-D networks can be written as

$$\begin{aligned} [X_T, Y_T] &= [P_{SVD}^{(2)}, P_{SVD}^{(3)}] \\ [X_T, Y_T, Z_T] &= [P_{SVD}^{(2)}, P_{SVD}^{(3)}, P_{SVD}^{(4)}] \end{aligned} \quad (8)$$

respectively.

While there are many possible ways to select the subset of nodes, we use the following two simple options in this paper:

- 1) Use the set of M anchor nodes ($Q=Q_A$)
- 2) Use a set of R randomly selected nodes ($Q=Q_R$)

As $N \gg M, R$, significant savings in overhead can be achieved, and results presented later demonstrate that the impact on accuracy is negligible.

V is a basis of R^M . V_Q is also a basis for R^M even though it is based on a subset of coordinates. Therefore, we can write $V = V_Q \cdot \Phi$, where Φ is a rotation matrix. If the selected subset of coordinates is a good representation of the entire P , similar TPMs can be generated as demonstrated in Section V, with significantly lower computational, memory and communication complexities.

A. A computationally efficient implementation

Computational power and memory available at a sensor node is limited. Conventional SVD calculation of $P_{N \times M}$, ($N \gg M$), which involves computing U , S and V , has approximately $(4N^2M + 8NM^2 + 9M^3)$ operations [13]. Also the memory requirement is approximately the sizes of V , U and S that is $(M \times M + N \times N + N \times M)$. In this section, we present a technique for further enhancing the efficiency of the computation necessary for 2-D and 3-D TPM generation. Note that U is a byproduct of SVD, and is not necessary for topology map computation. The Eigen-value decomposition (EVD) based approach [15] to evaluate matrix V not only allows us to implement the TPM generation in a distributed manner, but also completely avoids generating matrix U thus reducing the computational complexity and memory requirement compared to those for SVD. From (1), (3) and (4), $P_{SVD}^{(j)}$, the j^{th} column of P_{SVD} is given by

$$P_{SVD}^{(j)} = [h_{n_{iA_1}}, \dots, h_{n_{iA_M}}] \cdot V^{(j)}; i = 1:N \quad (9)$$

$[h_{n_{iA_1}}, \dots, h_{n_{iA_M}}]$ is the coordinate vector of the node i . Also $V^{(j)}$ is the j^{th} basis vector/column of V . $j = 2,3$ for 2-D networks, while $j = 2,3,4$ for 3-D networks. Thus, $V^{(2)}$ and $V^{(3)}$ are sufficient to evaluate 2-D Cartesian coordinates $[X_{T,i}, Y_{T,i}]$ of node i . 3-D networks require $V^{(2)}$, $V^{(3)}$ and $V^{(4)}$. Define C as

$$\begin{aligned} C &= P^T \cdot P = V \cdot S^2 \cdot V^T \\ C \cdot V &= V \cdot S^2 \end{aligned} \quad (10)$$

TABLE III. COMPUTATIONAL COMPLEXITY AND MEMORY USAGE COMPARISON

Method	Full SVD implementation with P	EVD method of estimating V of P
# Computations $N \gg M$	$(4N^2M + 8M^2 + 9M^3)$ [13]	Upper bounded by $(4M^2N + 8M^3)$ [13]
Memory usage	$(M \times M) + (N \times N) + (N \times M)$	Upper bounded by $(M \times M) + (1 \times M)$

IV. A METRIC FOR EVALUATING 2-D TOPOLOGY PRESERVATION

Evaluating the degree of topology preservation of the sensor node maps generated is essential for investigating the effectiveness of the proposed scheme. While visual inspection can provide preliminary evidence of its effectiveness, a formal metric is needed for quantifying the accuracy. A quantitative parameter to express the error provides a framework to compare and improve different mapping techniques. An effective metric should be able to capture and quantify the failures to preserve the topology of the real node map and the neighborhoods. Such a metric is not currently available. Here we develop a metric that can be used for this purpose.

A method based on coloring of nodes is used in [28] to show whether a neighborhood has been altered in the topology map. In [28] and [32], error is quantified as the difference of the positions in the actual physical map and the topology map, and the residual variance, respectively. The focus of our paper is TPMs based on hop distances. The requirement is that the map from calculated $[X_T, Y_T]$ set is homeomorphic to the physical layout, and preserves information about node connectivity, physical layout and physical voids. Thus the actual physical distance is not of significance, and the metrics in [28] and [32] are not appropriate.

Consider as an example, a 1-D network with 6 nodes numbered 1 to 6 as in Fig. 7(a). Figures 7(b) and (c) show two

C is a $M \times M$ symmetric matrix. This is an eigenvalue problem [15]. Therefore, let us solve,

$$C \cdot v = \lambda \cdot v \quad (11)$$

v is an eigenvector of C that is a column of V . Eigen values λ , can be found by solving

$$|C - \lambda \cdot I| = 0 \quad (12)$$

The eigenvectors corresponding to second and third *largest* eigenvalues provides the second and third columns of V . Now $[X_{T,i}, Y_{T,i}]$ ($[X_{T,i}, Y_{T,i}, Z_{T,i}]$ for 3-D case) can be evaluated locally without calculating the entire V matrix. Also $U_{N \times N}$ is not evaluated at all, which reduces the memory consumption significantly. Therefore the memory consumption is upper bounded by $(M \times M) + (1 \times M)$. Number of computations required for this method of calculating V is upper bounded by $(4M^2N + 8M^3)$ [13], which is the computations associated with calculation of entire V and S . Since $N \gg M$, this method is significantly less complex compared to the full SVD implementation (See Table III). For example, if the number of anchors in the network is set to $M \leq 0.01N$, which is reasonable based on our experience, the upper bound of computations required with this method is only 0.99% of the computations required for a full SVD based calculation with (3) and (4), indicating a significant reduction in complexity.

derived maps that need to be evaluated. If all the nodes are in same order as in initial topology then Topology Preservation Error must be 0%. Node 3 in Fig. 7(b) has flipped two node positions. The error metric should identify the number of out of order nodes as well as the degree of the error/node flips (one node and two node positions respectively for Fig. 7(b)).

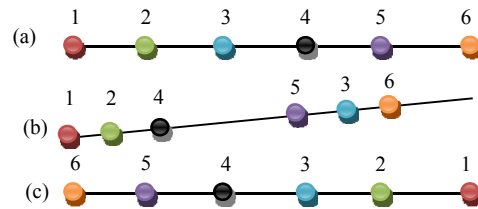


Fig. 7. (a) A network, (b) a topology map of (a) with a node flip, and (c) a topology map of (a) with 180° rotation.

Consider a 1D network with N nodes and define an indicator function $I_{i,j}$ where

$$I_{i,j} = \begin{cases} 1 & i \text{ and } j \text{ are out of order compared to original placement} \\ 0 & i \text{ and } j \text{ are in same order as original placement or } i = j \\ & i, j = 1 \text{ to } N. \end{cases}$$

Then, the number of out of order pairs is $\sum_{\text{all } i,j} (I_{i,j})$.

The total number of possible pairs in an N node network is P_2^N . We define the following metric:

$$\text{Topology Preservation Error} = E_{\text{TP}} = \frac{\sum_{\text{all } ij} (I_{ij})}{P_2^N} \quad (13)$$

For the network in Fig. 7(b), $N = 6$, and,

$$E_{\text{TP}} = (I_{3,4} + I_{3,5} + I_{4,3} + I_{5,3})/P_2^6 \times 100\% \\ = (I_{3,4} + I_{3,5})/C_2^6 \times 100\% = 13.3\%$$

Nodes 1 and 2 are in the right position compared to the rest while node 3 is shifted by 2 positions. Moreover, nodes 4 and 5 flipped their positions by 1. Therefore total node flips are 4 and E_{TP} is 13.3%. A TPM is invariant to rotations. Thus, for Fig. 7(c), where nodes are just reversed, E_{TP} has to be zero. To handle such cases, the two lines being compared need to be adjusted for any rotations.

To extend E_{TP} equation to 2-D topologies, we evaluate the 2-D topology by considering all contiguous line segments in two orthogonal directions (say \vec{H} and \vec{V}) of the physical map.

Let there be α lines in \vec{H} direction and β lines in \vec{V} direction in the network, then,

$$\text{Topology Preservation Error in } \vec{H} \text{ direction} = \\ E_{\text{TP}|\vec{H}} = \frac{\sum_{\alpha} \sum_{\text{all } ij} (I_{ij})}{\sum_{\alpha} P_2^{N_h}} \quad (14)$$

i, j are nodes in each horizontal line and each line has N_h nodes. Similarly, error in vertical direction is evaluated as Vertical neighborhood preservation error =

$$E_{\text{TP}|\vec{V}} = \frac{\sum_{\beta} \sum_{\text{all } ij} (I_{ij})}{\sum_{\beta} P_2^{N_v}} \quad (15)$$

i, j are nodes in each vertical line and each has N_v nodes. The overall Topology Preservation Error, E_{TP} , can be defined as:

$$E_{\text{TP}} = \frac{\sum_{\beta} \sum_{\text{all } ij} (I_{ij}) + \sum_{\alpha} \sum_{\text{all } ij} (I_{ij})}{\sum_{\alpha} P_2^{N_h} + \sum_{\beta} P_2^{N_v}} \quad (16)$$

V. RESULTS

The performance of the proposed TPM generation method is evaluated next using three 2-D examples and two 3-D examples representative of a variety of networks. MATLAB® 2009b was used for the computations.

A. TPMs of 2-D Networks

Figures identified as (a) in Fig. 8-10 show the physical maps of the three 2-D networks considered: An odd shaped network with 550 nodes (Fig. 8(a)), a 496-node circular shaped network with three physical voids/holes (Fig. 9(a)), and a network of 343 nodes on walls of a building (Fig. 10(a)). Communication range of a node in all three networks is unity. Detailed specifications of these networks are available at [4]. Topology maps are generated based on methods summarized in Table IV.

Unless otherwise indicated, the results shown correspond to fifteen randomly placed anchors in each of the networks. Building network in Fig. 10(a) has just three anchors. Fig. 8-10 (b) show TPMs constructed based on (4) using entire VC set of each network. Therefore TPMs in Fig. 8-10 (b) use input data matrices of sizes 550×15 , 496×15 and 343×3 respectively (Case 1, Table IV). Fig. 8-10 (c) are the topology maps created using only the anchors' coordinate set, that is using (7) and (8) based on the input data matrices Q_A of size 15×15 , 15×15 and 3×3 respectively (Case 2, Table IV). Topology maps in Fig. 8-10 (d) are created based on coordinates of 10 randomly selected nodes, i.e., the

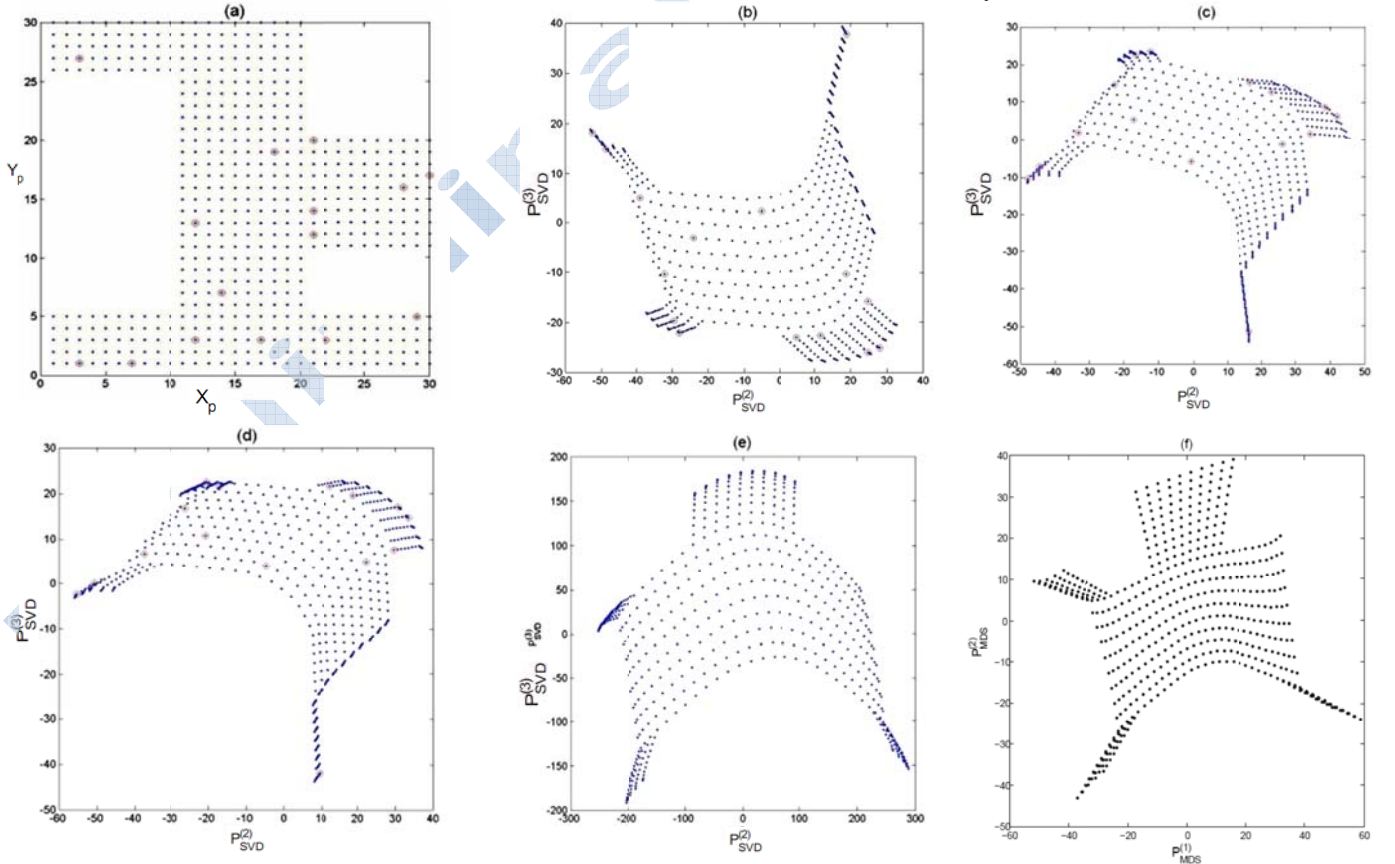


Fig. 8. a) Odd shaped network with 550 nodes and 10 random anchors; $[X_T, Y_T]$ is generated based on b) Case 1: entire VC set, c) Case 2: anchors' coordinate set, d) Case 3: randomly selected nodes' coordinate set, e) Case 4: coordinate set with all the nodes are anchors, and f) MDS.

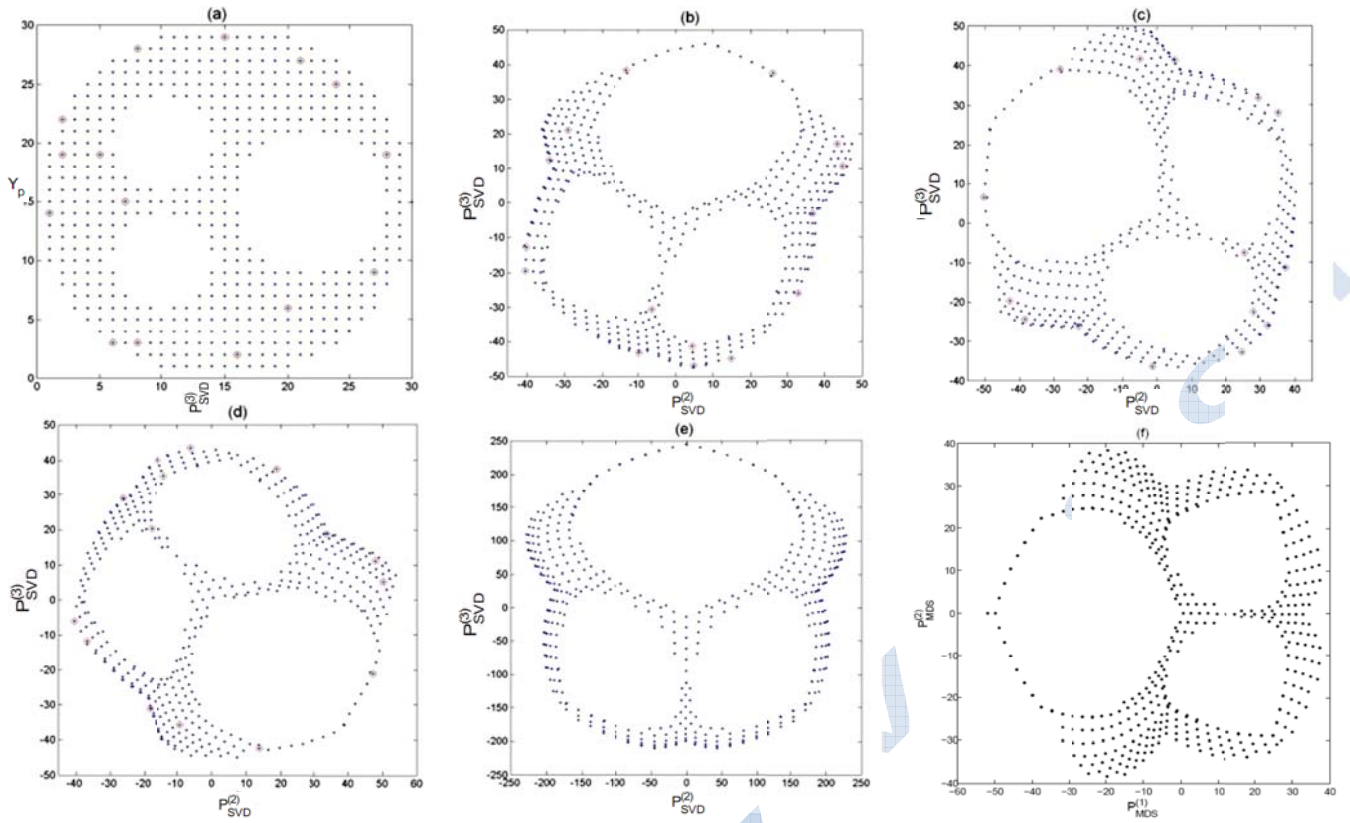


Fig. 9. a) Circular network with three physical voids with 496 nodes and 10 random anchors; $[X_T, Y_T]$ is generated based on b) Case 1- entire VC set, c) Case 2: anchors' coordinate set, d) Case 3: randomly selected nodes' coordinate set, e) Case 4: coordinate set with all the nodes are anchors, and f) MDS.

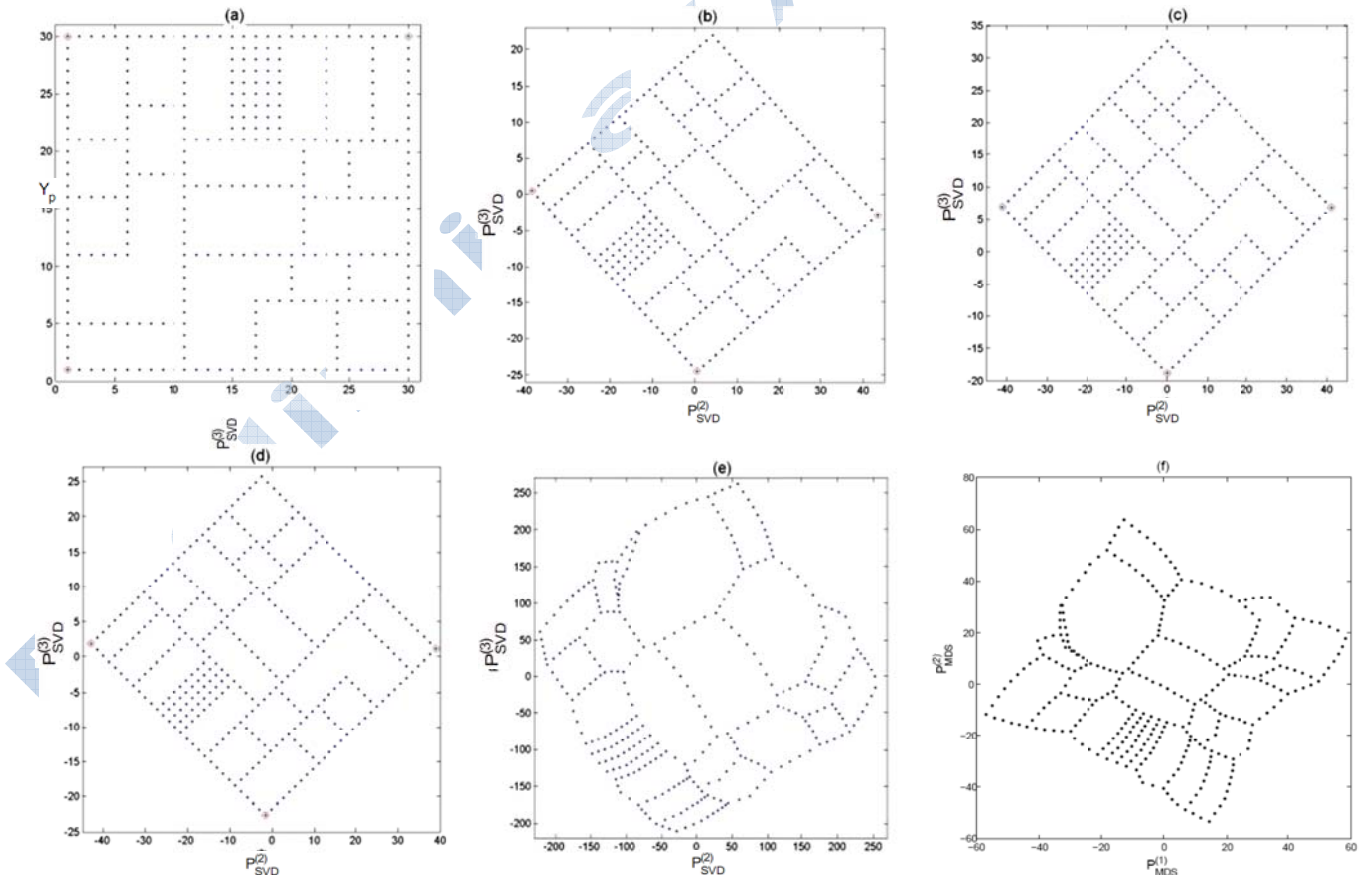


Fig. 10. a) Network in a building with 343 nodes and 3 anchors; $[X_T, Y_T]$ is generated based on b) Case 1- entire VC set, c) Case 2- anchors' coordinate set, d) Case 3- randomly selected nodes' coordinate set, e) Case 4- coordinate set with all the nodes are anchors, and f) MDS.

corresponding sizes of Q_R are 10×15 , 10×15 and 10×3 respectively (Case 3, Table IV). For the purpose of comparison, Fig. 8-10 (e) considers all the nodes in the network to be anchors, corresponding to P of sizes 550×550 , 496×496 and 343×343 respectively for the three networks (Case 4, Table IV). Case 3 is more efficient in terms of memory consumption and computational complexity. Finally, we compare our results with those of MDS-MAP method proposed in [29] shown in Fig. 8-10 (f). For MDS, data from the complete distance matrix D , which is defined as the matrix of all the pair-wise distances between points/nodes, is required. $D = [d_{ij}]_{N \times N}$, where, N is the number of nodes in the network and d_{ij} is the distance from node i to node j . As proposed in [29] d_{ij} can be either geodesic distance or hop distance between i and j . For this comparison we use hop distances to generate MDS-MAP, thus VCS requires all the nodes to be anchors. TPM for the circular network of Fig. 1(a) can be found in [9].

Figures 8-10 clearly demonstrate the effectiveness of the proposed method in generating TPMs. Starting just with VCs, without explicit knowledge of geographical information, the generated topology maps have captured significant features such as the physical voids and boundaries of the original network. A key observation we can draw from Fig. 8-10 is that the constructed topology maps are nonlinearly scaled and rotated compared to the actual network map. Yet, the original and constructed maps are topologically isomorphic. In contrast to previous cases, the topology maps of Fig. 10(b), (c), (d) are simply rotated and linear scaled versions of the original. In this network, we used only three anchors that were manually selected. The physical voids present in Fig. 10(a) are well preserved. Even though the map in Fig. 10(e) was obtained using all the nodes as anchors, its shape is deformed compared to Fig. 10(b)-(d), but in terms of neighborhood preservation Fig. 10(e) is better. For example, one of the L-shaped rooms in the building network (Fig. 10(a)) is distorted in the topology maps of Fig. 10(b)-(d). In Fig. 10(e) the L-shape is deformed but neighborhood of that L-shaped room is preserved. Case 4 is presented here only for the purpose of comparison. If all nodes are anchors, a very expensive proposition for WSNs, need for maps does not arise for many applications such as routing. Obtaining MDS-MAPs shown in Fig. 8-10 (f), require the hop distances from each node to every other node. A major disadvantage is that it is not feasible to implement MDS in a distributed manner due to the extremely high communication cost associated with generating the distance matrix consisting of distance between every pair of nodes. In fact, if such information is available at each node, it can be used to achieve 100% routability without the need to generate topology-preserving maps.

TABLE IV. FOUR DIFFERENT TOPOLOGY MAP GENERATION APPROACHES FOR WSNs OF N NODES AND M ANCHORS

Case	Description	Size of input data matrix
1	$[X_T, Y_T]$ from P	$N \times M$
2	$[X_T, Y_T]$ from Q_A	$M \times M$
3	$[X_T, Y_T]$ from Q_R	$R \times M$
4	$[X_T, Y_T]$ from $Q_A _{ A =M=N}$	$N \times N$

Moreover, from topology maps in Fig. 10, we can draw the valuable conclusion that a good anchor placement can significantly reduce the number of anchors required for topology map generation. It is topology preserving to a very high degree as intended. It can be clearly seen that maps in Fig. 10(b)-(d) are very close to the original map indicating that an appropriately placed small number of anchors can produce very accurate topology maps. This points to the possibility of obtaining even physically representative layout maps with appropriate selection of anchor nodes for a certain class of networks. Furthermore our later research in [22] demonstrates that TPMs can be obtained even under large communication ranges.

TABLE V. E_{TP} FOR TOPOLOGY MAPS IN FIG. 8-10.

Fig	E_{TP} (%)			
	Case 1	Case 2	Case 3	Case 4
Fig. 8 (a)	1.6777	1.5894	1.5011	1.4570
Fig. 9 (a)	0.3605	1.0698	0.4884	0
Fig. 10 (a)	0.1315	0.1315	0.1315	0.0376

E_{TP} (in (16)) for the different topology maps is presented in Table V. Note that the error in all the cases is less than 2%. The best performance in terms of E_{TP} was achieved when all the nodes were selected as anchors for the networks in Fig. 8-10. Case 4 (Table IV) acts as a lower bound for the E_{TP} for each network.

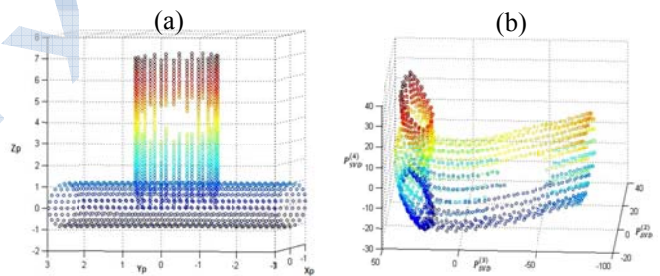


Fig. 11. 3-D Surface network, consisting of two perpendicular cylinders (T joint) (1642 nodes, 50 randomly selected anchors): a) Physical layout, and b) TPM.

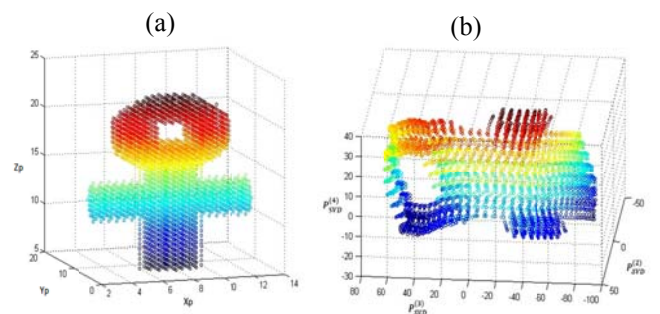


Fig. 12. 3-D Volume network, consisting of a sphere standing on two crossed cylinders. Sphere has a hole in it. (3827 nodes and 50 randomly selected anchors): a) Physical layout, and b) TPM.

Even though SVD based TPM generation started with a VC set where there is no directionality information, resultant topology map has directional information that can be used for routing in many ways. For example to avoid logical voids in VC routing, organized random routing and GR on TPM may be used [12]. Moreover, as discussed in Section II, there are

other VCSs [21][33], which are derivatives of hop distance based VCS used here. Use of the proposed TPM generation method with two such systems are addressed in Appendix B.

B. TPMs of 3-D networks

In this section we present the 3-D TPMs generated using the proposed scheme. Two example networks deployed on 3-D are considered as shown in Fig. 11 (a) and Fig. 12(a):

- T-joint (3-D surface network) - A pipeline structure joining two perpendicular cylinders in a T joint. There is a hole in one of the cylinders (see Fig. 11 (a)). Each cylinder has a unit radius and a height of 7 units. It is covered with 1642 nodes, each with a communication range of 0.4. 50 randomly selected nodes (i.e., 3% of the nodes) served as anchors.
- 3-D volume network - It consists of a solid sphere of radius 4 with a cylindrical hole, mounted on two perpendicularly crossed cylinders with height 10 and radius 2 (see Fig. 12 (a)). Entire volume is filled with 3827 nodes, each with a communication range of 0.5. 50 randomly selected nodes (i.e., less than 1.5% of the nodes) served as anchors.

TPMs of the corresponding physical topologies are shown in Fig. 11 and 12 respectively. The results clearly demonstrate the effectiveness of the TPM generation for sensor networks deployed on 3-D surfaces and in 3-D volumes. Moreover, it indicates that the maps can be obtained using a very small number of random nodes serving as anchors.

VI. REALIZATIONS, APPLICATIONS AND EXTENSIONS

The major contribution of this paper is the technique described and evaluated above for the generation of TPM. Subsection A, briefly addresses the realization details of the TPM algorithm in a static WSN. Routing is a crucial operation in WSNs. Subsection B discusses how WSN routing can benefit from TPMs. Subsection C discusses the impact of network dynamics on TPMs.

A. Off-network and In-network realization of TPM

First, let us consider the case where the TPM computation is done at a central node. There are many scenarios where a centralized implementation is feasible or even preferable. In a sensor network where the nodes are randomly deployed (e.g., dropped from a plane), it may be necessary and useful for the command center to obtain a map of the sensor node deployment indicating geographic voids, boundaries etc. In this case, each node may send information about its neighbors to a base or a central station. The adjacency matrix of the network is formed based on the nodes connectivity information, which can be gathered with the worst-case complexity of $O(N^2)$ where N is the number of nodes in the network. Then the procedures explained in Section III can be used to generate an effective and accurate TPM, since there is no computational or memory limitations at the base station. Moreover, if necessary, the map can be broadcast back to the individual nodes, together with the transformation matrix (V or V_Q), an operation of worst-case complexity of $O(N^2)$. Note that redistributing 2nd and 3rd columns of V or V_Q is sufficient for a node to calculate its topological coordinate. Generating

coordinates at a central station avoids multiple flooding in the network [5][6].

A distributed implementation of the above may be achieved as follows. The anchor based VC generation is first carried out the traditional way, i.e., via flooding. Following that, the anchors broadcast their coordinates, which requires $O(MN)$ messages. Since the sub-matrix ($Q=Q_A$) of all the anchors' coordinates is now available at each node, i , every node can generate V_Q (using (7)) and compute its own $[x_{T,i}, y_{T,i}]$ locally by simply multiplying its own coordinates by 2nd and 3rd columns of V_Q .

B. TPM based routing

We already asserted that in many ways the TPM is a better candidate for GR than the original physical map, as the former is based on actual connectivity information rather than the node position. A set of coordinates is good for routing if it results in accurate forwarding decisions. This can be quantitatively evaluated using

$$P[\text{Selecting correct neighbor}] = \frac{\# \text{ number of times a } N_j \text{ selected correct neighbor to FWD the packet when destination is } N_i}{\sum_{N_j \in N} \sum_{N_i \in N} \text{Total \# nodes (N)}} \quad (17)$$

Table VI shows this probability using physical and topology based Cartesian coordinates for two example networks. Topology maps generated with 10 randomly selected anchors have the capability of selecting the correct next neighbor as accurately as with physical coordinates for the networks in Fig. 9(a) and 10(a). Many other self-organization tasks can also be expected to perform well with TCs instead of geographical coordinates.

TABLE VI. PROBABILITY OF SELECTING THE CORRECT NEIGHBOR BASED ON TPM AND PHYSICAL MAP FOR THE NETWORKS IN FIG. 10

Network	Topology Maps				Physical Maps
	M=20	M=15	M=10	M=5	
Circle with voids (Fig. 10 a)	0.64	0.61	0.62	0.52	0.54
Building network(Fig. 9 a)	0.84	0.80	0.78	0.72	0.83

TABLE VII. PERFORMANCE COMPARISSION OF GLR, LCR, CSR AND GPSR WITH 10 ANCHORS [12]

Routing scheme	Avg. routability%	
	Circle with voids (Fig. 10 a)	Building network(Fig. 9 a)
GLR	94.6	89.3
LCR	56.5	49.7
CSR	87.3	75.4
GPSR	93.8	97.4

In static WSNs, the VC generation needs to be done less-frequently or perhaps only once during initialization. Therefore, topological coordinates also need not be updated frequently. Thus, the cost incurred in calculating Cartesian coordinates may be more than compensated by efficiency gains in terms of performance during long-term operation. For example, as illustrated in [12] the Geo-Logical Routing (GLR) scheme that uses both VCS and TPM to overcome disadvantages in each other's domains outperforms the physical information based routing scheme - Greedy Perimeter Stateless Routing (GPSR)[14]. Table VI summarizes the performance of GLR, the GC based scheme GPSR, and two

VCS based routing schemes, namely Convex Subspace Routing (CSR) and Logical Coordinate Routing (LCR). Routability is evaluated over all possible source-destination address pairs. Additional details of GLR algorithm are available in [12].

C. TPM for dynamic networks

Network dynamics that cause changes in connectivity among nodes pose a challenge for VC based approaches as VC values depend on the connectivity of the network. Examples of such conditions include node failures, the introduction of new nodes, and change in connectivity due to mobile nodes. TPMs presented here capture the physical layout information of the network, i.e., the topological coordinates corresponds to the physical position of a node, albeit on a somewhat distorted layout. When a node (or even an anchor) fails, the already calculated topology coordinates (TPCs) of a node still remain valid for the topology map. Thus, any algorithm relying on TPCs can continue to function even though the underlying VCs may no longer be valid. This can be considered as an advantage of using the TPCs instead of the VCs, as VCs have to be regenerated to accommodate the change in connectivity.

Introduction of new nodes or mobility of nodes that cause major changes in network topology can render the TPM inaccurate, thus requiring its re-computation. If the change in the connectivity pattern is completely localized, it may be possible to estimate the TCs of a new node based on some localized computations involving its immediate static neighbors.

VII. CONCLUSIONS AND FUTURE WORK

We presented a novel and a fundamental technique for generating TPMs from VCs for 2-D and 3-D (both surface and volume) WSNs. The transformation matrix for converting the virtual (logical) coordinates to a set of topological Cartesian coordinates can be obtained using the VCs of a very small set of nodes. Results show that a remarkable 2-D topology preservation error (E_{TP}) $\leq 2\%$ is achievable with a small number of anchors.

The topology coordinate space provides an alternative space for sensor networking algorithms beyond the traditional physical and VC spaces. It preserves the main advantage of VC scheme in not requiring distance measurements and that of GC scheme in having cardinal direction and boundary/void information. TPMs may be used in lieu of physical maps for many applications and WSN protocols [12]. The TPM generation scheme presented above has been used for functions such as boundary node identification, event region and void detection [10] with performance on par with GC based schemes. In fact, the topological coordinates (TCs) in conjunction with VCs from which they are derived, have been demonstrated to be better than geographical coordinates for routing with significantly enhanced routing performance [12]. While there are certain applications for which the exact sensor location is necessary, for others that do not need such information, TPM presents a robust, accurate and a scalable alternative to physical map generation or localization. Sensor network applications of TPMs are diverse and vast; examples include routing, localization, boundary node identification, and effective anchor placement.

We envision many applications of the proposed topology preserving map extraction methodology in other types of networks as well as in multidimensional graphs, e.g., for dimension reduction, visualization and information extraction. Methods to compensate for the distortion of the maps compared to physical maps, and techniques that use derived Cartesian coordinates and the topology map to improve self-organization and routing protocols are also under investigation.

ACKNOWLEDGEMENTS

This research was supported in part by NSF Grant CNS 0720889.

ACKNOWLEDGEMENTS

This appendix addresses the convexity of first principle component of an anchor based VCS and the applicability of proposed TPM generation scheme for other existing VCSs.

A. Convexity of the first principle component

Being the distance to the corresponding anchor from a node, by definition each VC radially increases around the corresponding anchor. Due to the fact that 1st principle component (PC) captures the salient dominant features of the dataset, its magnitude variation over the network is always convex; due to the possibility of having positive or negative sign, the actual shape of 1st PC variation is either convex or concave.

We demonstrate the convexity of magnitude first on a simple 1-D network, and then extend it to a 2-D full grid. Let the VCS with respect to M anchors of a 1-D network, as illustrated in Figure A.1(a), be $P = [P^{(1)} P^{(2)} \dots P^{(M)}]$. By definition each VC with respect to anchor A_j : $P^{(j)}$ is a convex function with respect to the node position n_i . The 1st PC can be written as:

$$P_{SVD}^{(1)} = [P^{(1)} P^{(2)} \dots P^{(M)}] \cdot V^{(1)} \quad (A.1)$$

$PV^{(1)}$, is a linear combination of the set of convex functions $P^{(j)}$ s. Reference [24] proves that the direction of 1st PC, i.e. $V^{(1)}$, goes through the centroid of the data points. Since, $P^{(j)}$ lie in the 1st orthant of the multidimensional space all the time, its centroid is also in the 1st orthant. Hence $V^{(1)}$ is a unit vector with either all positive coefficient or all negative coefficients. Without loss of generality one can say, Eq. (A.1) is the addition of M convex functions and thus 1st PC is also a convex function. For the example in, variation of 1st and 2nd PCs are shown in Fig. A.1(b). The 1-D maps of the network obtained using 1st PC (Fig. A.1(c)) shows a network that is folded in two as expected, that using 2nd PC (Fig A.1(d)) shows a map where topology and local neighborhoods are preserved.

A similar argument can be made for the 2-D full grid, since VCs with respect to anchor A_i is a 2-D convex surface. Moreover, all the ordinates lie in the 1st orthant. Hence for a 2-D grid $V^{(1)}$ is a unit vector with either all positive or all negative coefficients resulting in a sum of convex functions, which is convex. Therefore, 1st PC is convex for a 2D full grid as well. Figure A.2(a) shows the map of the network of Fig.

1(a) when the 1st and 2nd PCs are used as axis. The network gets folded due to the dominant convex shape of the 1st PC. In contrast, the map in Fig A.2(b) using 2nd and 3rd PCs as axis is a TPM that preserves local neighborhoods.

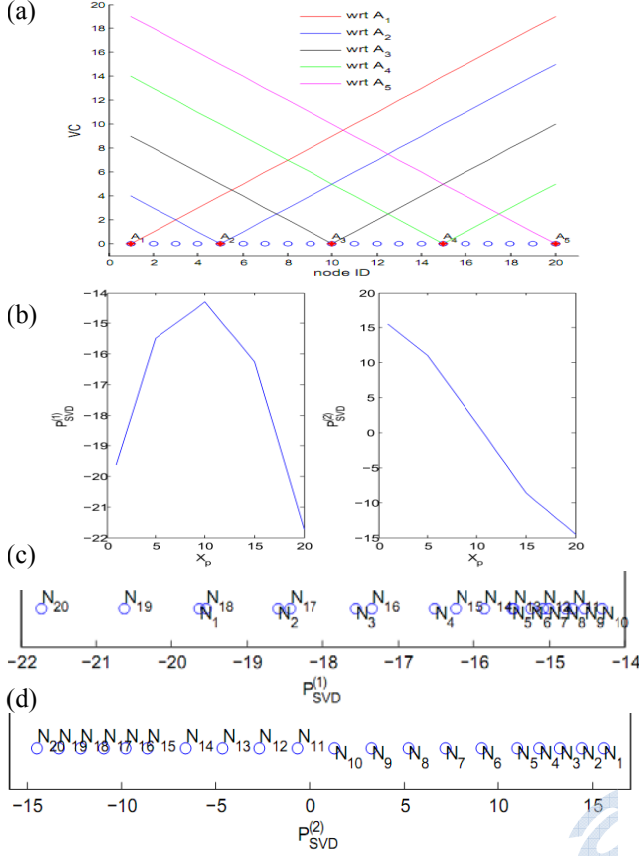


Figure A.1: (a) VCS corresponding to two anchors in a 1D network. (b) 1st and 2nd PCs for the VCS in (a), (c) TPM of the network in (a) based on 1st PC, and (d) TPM of the network in (a) using 2nd PC.

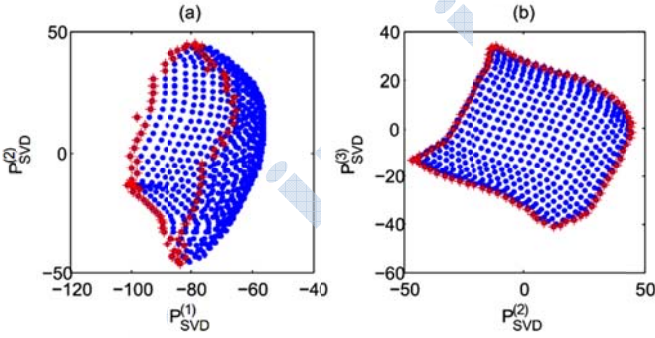


Figure A.2. Topology Preserving Map of a circular network (Fig. 1(a)) using (a) 1st and 2nd PC (b) 2nd and 3rd PC. The edge nodes of the network are highlighted.

A. TPM from other virtual coordinate systems

The use of proposed TPM generation technique with other VCSs derived from hop distances is demonstrated next using two such schemes, ABVCap[33] and Aligned VCS[21].

Axis Based VC Assignment protocol (ABVCap)[33] characterizes each node by a five tuple consisting of (longitude, latitude, ripple, up, down). These entries are specified relative to virtual lines identified in the network as follows. Initially, three anchors (X, Y, Z) are selected based on

VCap anchor selection. A fourth anchor, Z', is selected such that it is furthest away from Z and equidistance from X and Y. Generation of 5-tuple (longitude, latitude, ripple, up, down) involves several additional network floodings. Figure B.1 (a) shows an example network used in [33] with ABVCap-VCS.

One notable property of ABVCap-VCS is that some nodes have more than one VC tuple assigned to them. Either one of the tuples has to be selected for each node, which introduces unnecessary complexity to identify the proper tuple for topology map generation, or multiple positions in TPM will be assigned to the same node based on different coordinate tuples. The TPM shown in Fig. B.1 (b) is generated using our scheme based on VC tuples identified in bold in Fig. B.1 (a). Figure B.1 (c) indicates multiple positions created for node 12 due to its multiple coordinates in ABVCap. As ABVCap based VCS does not have concentricity increasing property, 1st PC and 2nd PC provide the TPM. While this demonstrates the applicability of TPM for ABVCap, we note that essentially the same information can be obtained simply by applying the method to a simple VCS without having to undergo overhead required to generate ABVCap.

Aligned VCS [21] proposes a modification for VCS to alleviate the local minima problem simply by replacing the VCs of each node with the average of node's and its neighbors' VCs. Thus we have used the VCS w.r.t (X, Y, Z, Z') of Fig. B.1 (a) to evaluate aligned VCS as in [21]. The TPM from the corresponding aligned VCS is shown in Fig. B.1 (d). Since aligned VCs are also radial in nature, the radial component can be removed using the 1st PC, and the 2nd and 3rd PCs provide the Cartesian coordinates. These results indicate the applicability of the proposed TPM generation technique to other VCS as well.

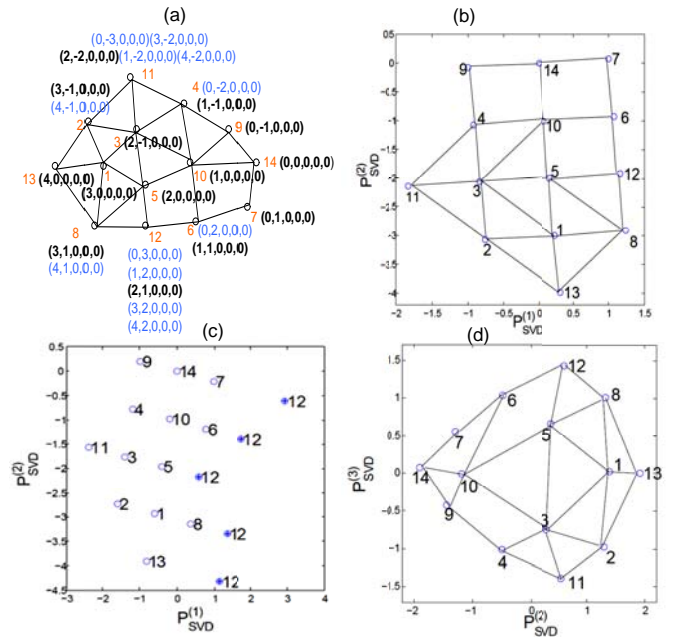


Figure B.1: (a) An example network with its ABVCap VCS [33], (b) TPM only with ABVCap coordinates in bold black, (c) TPM with all possible ABVCap coordinates of node 12, and (d) TPM from Aligned VCs.

REFERENCES

[1] I. F. Akyldi and J. M. Jornet, "The Internet of Nano-Things," IEEE Wireless Communication Networks, Dec. 2010.

- [2] J. Bachrach and C. Taylor, "Localization in sensor networks," Ch. 9, Handbook of Sensor Networks, Stojmenovic (Editor), John Wiley 2005.
- [3] Y. Bengio, J-F. Paiement, P. Vincent, "Out-of-sample extensions for l1e, Isomap, MDS, eigenmaps, and spectral clustering," In Advances in Neural Information Processing Systems, 2003
- [4] CSU Sensor-Net Benchmarks, Available: <http://www.cnrl.colostate.edu/Projects/VCS/>
- [5] A. Caruso, S. Chessa, S. De, and A. Urpi, "GPS free coordinate assignment and routing in wireless sensor networks," Proc. INFOCOM 2005, Vol. 1, pp. 150- 160, Mar. 2005.
- [6] Q. Cao and T Abdelzaher, "Scalable logical coordinates framework for routing in wireless sensor networks," ACM Transactions on Sensor Networks, Vol. 2, pp. 557-593, Nov 2006.
- [7] D.C. Dhanapala, "On performance of random routing and virtual coordinate based routing in WSNs", M.S. Thesis, Colorado State University, Fort Collins, CO, USA, 2009.
- [8] D. C. Dhanapala and A. P. Jayasumana, "CSR: convex subspace routing protocol for WSNs," Proc. 33rd IEEE Conf. on Local Computer Networks, Oct. 2009.
- [9] D.C. Dhanapala and A.P. Jayasumana, "Topology preserving maps from virtual coordinates for wireless sensor networks," Proc. 35th IEEE Conf. on Local Computer Networks (LCN 2010), Oct. 2010.
- [10] D.C. Dhanapala, S. Mehta and A.P. Jayasumana, "Boundary detection of sensor and nanonetworks deployed on 2-d and 3-d surfaces," IEEE Globecom - Ad-hoc and Sensor Networking Symposium, 2011.
- [11] D.C. Dhanapala and A.P. Jayasumana, "Clueless Nodes to Network-Cognizant Smart Nodes: Achieving Network Awareness in Wireless Sensor Networks" IEEE CCNC 2012.
- [12] D.C. Dhanapala and A.P. Jayasumana, "Geo-Logical Routing in wireless sensor networks," Proc. 8th IEEE Communications Society Conf. on Sensor, Mesh and Ad Hoc Communications and Networks (SECON), June 2011.
- [13] R. Hartley and A. Zisserman, "Multiple view geometry in computer vision," Appendix 4, 2nd Edition, Cambridge University Press New York, 2003.
- [14] B. Karp and H. T. Kung., "Greedy Perimeter Stateless Routing (GPSR) for wireless networks," Proc. 6th ACM/IEEE Int. Conf. on Mobile Computing and Networking (Mobicom), 2000, pp. 243-254.
- [15] M. Kirby, "Geometric data analysis - An empirical approach to dimensionality reduction and the study of patterns," John Wiley & Sons, 2001.
- [16] F. Kuhn, R. Wattenhofer, Y. Zhang, and A. Zollinger, "Geometric ad-hoc routing: of theory and practice," Proc. 22nd ACM Int. Symposium on the Principles of Distributed Computing (PODC), July 2003.
- [17] S. Lederer, Y. Wang and J. Gao; "Connectivity-Based Localization of Large Scale Sensor Networks with Complex Shape," Proc. 27th IEEE INFOCOM, 2008, pp: 789 - 797.
- [18] B. Leong, S. Mitra, and B. Liskov, "Path vector face routing: geographic routing with local face information," 13th IEEE Int. Conf. on Network Protocols (ICNP), Nov. 2005.
- [19] K. Lferd, J.R. Martínez-de Dios, A. de San Bernabé, and A. Ollero, "Experimental comparison of RSSI and TOF measurements for localization," Proc. European Conference on Wireless Sensor Networks (EWSN), Poster, 2011.
- [20] O. Liang; Y.A. Sekercioglu, and N. Mani, "A Low-Cost Flooding Algorithm for Wireless Sensor Networks," IEEE Wireless Communications and Networking Conference, pp. 3495 - 3500, March 2007.
- [21] K. Liu and N. Abu-Ghazaleh, "Aligned virtual coordinates for greedy routing in WSNs," Proc. IEEE Int. Conf. on Mobile Adhoc and Sensor Systems, pp. 377-386, Oct. 2006.
- [22] S. Mehta, "Evaluation of topology generation in sensor networks," MS Project Report, Colorado State University, CO, USA, 2011.
- [23] N. Mitton, T. Razafindralambo, D. Simplot-Ryl and I. Stojmenovic, "Hector is an Energy efficient Tree-based Optimized Routing protocol for wireless networks," Proc. Int. Conf. on Mobile Ad-hoc and Sensor Networks (MSN), Dec. 2008.
- [24] K. Pearson, "On lines and planes of closest fit to systems of points in space," Philosophical Magazine, 1901, pp: 559-572.
- [25] H.A.B.F. Oliveira, E. F. Nakamura, A. A. F. Loureiro, and A. Boukerche, "Error analysis of localization systems for sensor networks," Proc. 13th ACM Int. Workshop on Geographic Information Systems, New York, USA, 2005
- [26] J. Polastre, R. Szewczyk, and D. Culler, "Telos: Enabling Ultra-Low Power Wireless Research," 4th Int. Symposium on Information Processing in Sensor Networks (IPSN 2005), 15 April 2005, pp. 364 - 369.
- [27] A. Rao, S. Ratnasamy, C. Papadimitriou, S. Shenker, and I. Stoica, "Geographic routing without location information," Proc. 9th Int. Conf. on Mobile Computing and Networking, pp. 96 - 108, 2003.
- [28] S. T. Roweis, and L. K. Saul, "Nonlinear dimensionality reduction by locally linear embedding," Science, Vol 290, pp: 23239-2326, 22 Dec. 2000.
- [29] Y. Shang, W. Ruml, Y. Zhang and M. Fromherz, "Localization from connectivity in sensor networks," IEEE Transactions on Parallel and Distributed Systems (2004), pp. 961-974.
- [30] J. A. Sanchez, P. M. Ruiz, "Exploiting Local Knowledge to Enhance Energy-Efficient Geographic Routing," Lecture Notes in Computer Science, Vol. 4325, Dec. 2006, pp. 567-578.
- [31] M. Steyvers, "Multidimensional scaling," Encyclopedia of Cognitive Science, 2002.
- [32] J. B. Tenenbaum, V. de Silva and J. C. Langford, "A global geometric framework for nonlinear dimensionality reduction," Science, Vol 290, pp: 2319-2323, 22 Dec. 2000.
- [33] M. J. Tsai, H. Y. Yang, and W. Q. Huang, "Axis based virtual coordinate assignment protocol and delivery guaranteed routing protocol in wireless sensor networks," Proc. INFOCOM 2007, pp: 2234-2242, May 2007.
- [34] Y. Yu, R. Govindan and D. Estrin, "Geographical and energy aware routing: a recursive data dissemination protocol for WSNs," UCLA CS Dept Tech. Rept., UCLA/CSD-TR-01-0023, May 2001.
- [35] H. Zhou, H. Wu, S. Xia, M. Jin, and N. Ding, "A distributed triangulation algorithm for wireless sensor networks on 2D and 3D surface," Proc. IEEE INFOCOM, 2011, pp: 1053 - 1061.



Dulanjale C. Dhanapala received her bachelor's degree, with First Class Honors in Electrical and Electronics Engineering from University of Peradeniya, Sri Lanka in 2006. She completed her M.S. in Electrical and Computer Engineering at Colorado State University, USA, in 2009. She is currently working towards completing the Ph.D. degree from the Department of Electrical and Computer Engineering at Colorado State University. Her research interests include wireless sensor networks, communication networks, communication theory, and digital communication.



Anura P. Jayasumana is a Professor in Electrical & Computer Engineering and Computer Science at Colorado State University. He received Ph.D. and M.S. in Electrical Engineering from Michigan State University, and B.Sc. in Electronic and Telecommunications Engineering with First Class Honors from University of Moratuwa, Sri Lanka. His current research interests include sensor networking, network protocols, and

performance modeling. Anura also serves as a consultant to industry; his past clients range from startups to Fortune 100 companies. He is a member of Phi Kappa Phi, ACM and IEEE.